Fluid Phase Equilibria 496 (2019) 80–92

Contents lists available at ScienceDirect

Fluid Phase Equilibria

journal homepage: www.elsevier.com/locate/fluid

Effective Hamiltonians and empirical fluid equations of state

Roman Tomaschitz

Sechsschimmelgasse 1/21-22, A-1090, Vienna, Austria

ARTICLE INFO

Article history:
Received 14 March 2019
Received in revised form
15 May 2019
Accepted 19 May 2019
Available online 22 May 2019

Keywords:
Non-cubic equations of state
Classical and quantum fluids
Effective partition function
Equilibrium entropy and internal energy
High-pressure regime
Critical, sub- and supercritical isotherms

ABSTRACT

Hamiltonians with explicit temperature and density dependence are employed in classical and quantized partition functions to derive caloric and thermal equations of state (EoS) for real gases and liquids. To define a fluid equilibrium system, the density- and temperature-dependent Hamiltonian has to satisfy an equilibrium condition derived here, which ensures that the internal-energy derivative of entropy coincides with the reciprocal temperature. The inverse problem to obtain an effective Hamiltonian from a prescribed thermal EoS is discussed, and explicit examples of this reconstruction are given for cubic and non-cubic EoSs. A non-cubic multi-parameter EoS is proposed, a generalization of the Peng-Robinson EoS, which can accurately reproduce the power-law ascent of pressure isotherms in the high-pressure/high-density regime. This EoS is put to test by fitting isothermal data sets of classical and quantum fluids (nitrogen, carbon monoxide, methane, carbon dioxide, methanol, water, hydrogen and helium) over an extended pressure range up to 1 GPa, at critical, super- and subcritical temperatures. The least-squares fits are compared with the cubic Peng-Robinson approximation of the pressure isotherms, which becomes singular at high density. The internal-energy variable derived from the effective Hamiltonian can also be used to discriminate between different EoSs in the high-density regime, as demonstrated with methane isotherms.

© 2019 Elsevier B.V. All rights reserved.

1. Introduction

Starting with an empirical equation of state (EoS), we show how to obtain an effective Hamiltonian which defines the partition function of an equilibrium system and reproduces the prescribed thermal EoS. The formalism developed is motivated by the Debye-Hückel theory of dilute plasmas and electrolytes [1–3]. In this theory, the Coulomb potential is turned into a short-range interaction by adding an exponential screening factor. The exponent of this cutoff factor is explicitly depending on temperature and particle density. To evaluate the partition function, the screened Coulomb potential is expanded in an ascending power series in the radial coordinate, and only the second term thereof, which is independent of the radial coordinate, is retained.

In effect, the Coulomb potential of the Hamiltonian is replaced by a constant independent of the radial coordinate but depending on temperature and particle density, since the exponent of the cutoff factor depends on these variables. In this approximation, the partition function can be evaluated in closed form, as well as the entropy function and the internal energy. Since the Hamiltonian is explicitly temperature and density dependent, the internal-energy derivative of entropy does not exactly coincide with the inverse temperature, which is a basic requirement of an equilibrium system, but contains some additional terms. These terms become negligible in the low-density regime, so that the density- and temperature-dependent Hamiltonian of the Debye-Hückel theory still defines an equilibrium system at low density, suitable to model dilute electrolytes [3].

Here, we consider a more general context, fluid equations of state empirically obtained, and reconstruct the effective temperature- and density-dependent Hamiltonian reproducing the prescribed EoS. In contrast to the Debye-Hückel theory, a low-density approximation is not assumed. In fact, the formalism is designed to be efficient at high pressure and high density, where virial/fugacity expansions fail. Since the Hamiltonian is density and temperature dependent, it has to satisfy an equilibrium condition for the partition function to define an equilibrium entropy. Explicit examples of effective Hamiltonians are given for cubic equations of state such as the Peng-Robinson (PR) EoS and Soave-Redlich-Kwong (SRK) EoS, cf. Refs. [4,5] for reviews of these equations. The general reconstruction method of effective Hamiltonians and partition functions, applicable to non-cubic EoSs, is also explained and tested with a multi-parameter EoS.

E-mail address: tom@geminga.org.

https://doi.org/10.1016/j.fluid.2019.05.014
0378-3812/© 2019 Elsevier B.V. All rights reserved.

A non-cubic multi-parameter EoS is introduced, distinguished from cubic EoSs by a non-singular repulsive term. Isothermal high-pressure/high-density data sets [6] of several classical and quantum gases/liquids are considered, and least-squares fits of the proposed EoS to critical, sub- and supercritical pressure isotherms are performed. The fitted isotherms are compared with approximations obtained with the cubic PR EoS which predicts a singularity in the pressure isotherms at high density, whereas the proposed EoS reproduces the power-law ascent observed in isothermal data sets above the critical density and manifested by nearly straight power-law slopes in log-log plots.

The PR and SRK equations depend on an empirical function of temperature in the attractive term of the EoS. This 'alpha function' is parametrized with the acentric factor of the fluid. There is a vast body of literature on attempts to find a simple analytic expression of this function, e.g., Refs. [7–20]. Typically, a specific analytic temperature dependence is assumed with a constant depending on the acentric factor ω. This constant is assumed to be a polynomial in ω with coefficients to be determined by regression analysis based on a large number of compounds, see Refs. [21,22] for recent estimates. A variety of alpha functions suggested over the years is listed in Table 4-7 of Ref. [4] and Table 1 of Ref. [5].

In the low and intermediate density and pressure regime, the PR and SRK equations endowed with up-to-date alpha functions [22] are quite efficient to predict thermodynamic variables over a wide temperature and ω range, especially for engineering applications. However, their ability to reproduce high-pressure data sets is limited, even qualitatively, as will be demonstrated in this paper. As mentioned, the non-cubic multi-parameter EoS proposed here has a repulsive term which stays regular at high density, so that high-pressure/high-density data sets can be reproduced with good precision, and the same holds true for the internal energy at high density. The basic prediction is that the pressure isotherms are singularity free at high density, with power-law increase beyond the density limit suggested by cubic equations.

Non-cubic equations of state like the modified Benedict-Webb-Rubin EoS [23,24], Wagner EoS [25,26], SAFT EoS [27] and GERG-2008 EoS [28] contain a large number of terms, sometimes motivated by high-order virial expansions. These multi-parameter EoSs can be marred by consecutive Maxwell loops in the two-phase region [29]. Despite the fact that the proposed non-cubic EoS is a multi-parameter equation, the subcritical pressure isotherms safely admit only one Maxwell loop (defined by a unique local maximum followed by a minimum in the coexistence region), since the EoS is structurally close to a cubic equation, consisting only of an attractive and repulsive term.

In the remainder of this section, we give an outline of the paper. In Section 2.1, classical partition functions are studied, defined by an effective Hamiltonian depending on temperature and particle density. The caloric and thermal equations of state are derived, by employing the equilibrium condition satisfied by the effective Hamiltonian. In Section 2.2, the inverse problem is considered: based on a prescribed thermal EoS, the effective Hamiltonian defining the EoS is reconstructed. Analytically solvable examples are given, by calculating the effective Hamiltonians of the van der Waals, PR and SRK EoSs. In Section 3, the equilibrium condition for a temperature- and density-dependent Hamiltonian is derived, applicable to classical and quantized partition functions.

In Section 4.1, a non-cubic EoS is introduced by adapting the repulsive and attractive terms of the PR EoS to high-pressure/high-density data sets. The repulsive term is singularity free and the EoS is capable of reproducing the power-law slopes emerging at high density in double-logarithmic plots of the pressure isotherms. The EoS also accurately reproduces the isotherms in the vicinity of the critical point. In Section 4.2, the PR and SRK EoSs are shown to be special cases of the proposed non-cubic EoS, obtained by suitably specifying the amplitudes and exponents which are otherwise fit parameters of the EoS.

In Section 4.3, the critical, super- and subcritical pressure isotherms of classical and quantum gases/liquids (nitrogen, carbon monoxide, methane, carbon dioxide, methanol, water, hydrogen and helium) are studied, and least-squares fits of the proposed EoS to isothermal data sets [6] are performed, which extend over several orders in pressure up to 1 GPa. The temperature dependent amplitudes and power-law exponent defining the attractive term of the EoS are treated as temperature dependent fitting parameters rather than as analytic functions. The fits are compared with the PR approximation which predicts a singularity in the pressure isotherms at high density.

In Section 4.4, the temperature evolution of pressure isotherms is studied in the vicinity of the critical temperature. Power series expansions are employed to model the temperature dependence of the EoS. That is, the temperature dependent exponent and amplitudes of the EoS are specified as analytic functions. A specific example, the EoS of water, is worked out. The power series coefficients are inferred from least-squares fits, using data sets obtained in Section 4.3 from water pressure isotherms.

This paper focuses on pressure isotherms at high density. In Section 5, we also discuss the internal energy derived from cubic and non-cubic EoSs by way of their effective Hamiltonian. In particular, the internal energy of methane at critical, sub- and supercritical temperatures is studied. At high density, qualitative differences emerge in the internal-energy isotherms obtained from cubic and non-cubic equations, which are subjected to test by comparison with high-density data sets of methane. Section 6 summarizes the results and conclusions.

2. Classical statistics with temperature- and density-dependent Hamiltonian

2.1. Effective partition function, thermal and caloric equations of state

We consider the classical spectral density

$$\mathrm{d}\rho(p) = \frac{4\pi\sigma}{(2\pi)^3}\mathrm{e}^{-\alpha-\beta H(p;T,n)}p^2\mathrm{d}p \tag{2.1}$$

where the effective Hamiltonian $H(p;T,n)$ depends on the particle momenta p, temperature and particle density $n = N/V$ [30–32]. σ is the spin degeneracy, α the fugacity parameter, and $\beta = 1/T$. ($\hbar = k_\mathrm{B} = 1$.) The particle density, internal energy density $u = U/V$, partition function Z and the spectral density are related by the general equilibrium identities

$$n = -\frac{(\log Z)_{,\alpha}}{V} = \int_0^\infty \mathrm{d}\rho(p) \tag{2.2}$$

$$u = -\frac{(\log Z)_{,\beta}}{V} = \int_0^\infty H(p;T,n)\mathrm{d}\rho(p) \tag{2.3}$$

The identity $\xi := \log Z/V = n$ holds as well, based on the classical spectral density (2.1).

The effective Hamiltonian in (2.1) is specified as

$$H(p;T,n) = g(T,n)p^2 + h(T,n) \tag{2.4}$$

where $g(T,n)$ and $h(T,n)$ are arbitrary functions of temperature and

density. The integrals in (2.2) and (2.3) are then elementary:

$$n=\frac{4\pi\sigma}{(2\pi)^3}\mathrm{e}^{-\alpha-h(T,n)/T}\frac{\sqrt{\pi}}{4}\frac{1}{(g(T,n)/T)^{3/2}} \tag{2.5}$$

$$u=h(T,n)n+g(T,n)\frac{4\pi\sigma}{(2\pi)^3}\mathrm{e}^{-\alpha-h(T,n)/T}\frac{\sqrt{\pi}}{4}\frac{3}{2}\frac{1}{(g(T,n)/T)^{5/2}} \tag{2.6}$$

Solving Eq. (2.5) for α and introducing the shortcut $\tilde{g}(T,n)=\log(2mg(T,n))$, where m is the particle mass, we obtain

$$\alpha(T,n)=\frac{3}{2}\log T-\frac{3}{2}\tilde{g}(T,n)-\log n-\frac{h(T,n)}{T}+\log\left(\frac{\sqrt{\pi}}{4}\frac{4\pi\sigma}{(2\pi)^3}\right)+\frac{3}{2}\log(2m) \tag{2.7}$$

Substituting this into (2.6), the internal energy density $u=U/V$ (caloric EoS) becomes

$$u(T,n)=h(T,n)n+\frac{3}{2}nT \tag{2.8}$$

and the derivatives of $u(T,n)$ and the fugacity parameter read

$$u_{,T}=h_{,T}n+\frac{3}{2}n,\quad u_{,n}=h+h_{,n}n+\frac{3}{2}T \tag{2.9}$$

$$\alpha_{,T}=\frac{3}{2}\frac{1}{T}-\frac{3}{2}\tilde{g}_{,T}-\frac{h_{,T}}{T}+\frac{h}{T^2},\quad \alpha_{,n}=-\frac{3}{2}\tilde{g}_{,n}-\frac{1}{n}-\frac{h_{,n}}{T} \tag{2.10}$$

In Section 3, we will derive the equilibrium condition $\xi_{,T}-u/T^2+\alpha_{,T}n=0$ (with $\xi=\log Z/V$) in a more general context also applicable to quantum systems, cf. (3.12). This is a necessary and sufficient condition ensuring that the internal-energy derivative of entropy is the inverse temperature, $S_{,U}=1/T$. For a classical fluid system (2.1), (2.4), this condition simplifies to

$$h_{,T}(T,n)+\tilde{g}_{,T}(T,n)\frac{3}{2}T=0 \tag{2.11}$$

since in this case $\xi=n$, cf. after (2.3) and (2.8), (2.10). The otherwise arbitrary functions $h(T,n)$ and $g(T,n)=\mathrm{e}^{\tilde{g}(T,n)}/(2m)$ in Hamiltonian (2.4) have to satisfy this condition for the spectral density (2.1) to define an equilibrium system.

The thermal equation of state $P=T(\xi-\xi_{,n}n-\alpha_{,n}n^2)$, derived in Section 3, is based on a classical or quantized partition function defined by an effective Hamiltonian $H(p;T,n)$ depending on temperature and particle density, cf. (3.13). For a classical system specified by the spectral density (2.1) and Hamiltonian (2.4) subject to the equilibrium condition (2.11), this EoS and its temperature derivative can be written as

$$P=Tn+n^2\left(h_{,n}+\frac{3}{2}\tilde{g}_{,n}T\right),\ P_{,T}=n+\frac{3}{2}\tilde{g}_{,n}(T,n)n^2 \tag{2.12}$$

where we used again the classical identity $\xi=n$ and (2.10). Similarly, the chemical potential $\mu=-T(\xi_{,n}+\alpha+\alpha_{,n}n)$ derived in (3.13) simplifies for a classical system (2.1), (2.4), (2.11) to

$$\mu=-T\alpha+n\left(h_{,n}+\frac{3}{2}\tilde{g}_{,n}T\right) \tag{2.13}$$

with the fugacity parameter $\alpha(T,n)$ in (2.7) substituted.

The isochoric heat capacity $C_V=Vu_{,T}$ is defined by $u_{,T}$ in (2.9), and the specific entropy density $S/V=s(T,n)=\xi+\alpha n+u/T$, cf. (3.7), is assembled from (2.7) and (2.8),

$$s=n\left[\frac{3}{2}\log T-\frac{3}{2}\tilde{g}(T,n)-\log n+\log\left(\frac{\sqrt{\pi}}{4}\frac{4\pi\sigma}{(2\pi)^3}\right)+\frac{3}{2}\log(2m)+\frac{5}{2}\right] \tag{2.14}$$

The Helmholtz free energy, $F=(u-Ts)V$, can be assembled from (2.8) and (2.14).

2.2. Reconstruction of the effective Hamiltonian from an empirical thermal EoS

Based on a prescribed equation of state $P(T,n)$, an effective Hamiltonian $H=g(T,n)p^2+h(T,n)$, $g(T,n)=\mathrm{e}^{\tilde{g}(T,n)}/(2m)$, cf. (2.4), can be found which satisfies the equilibrium condition (2.11) and defines the spectral density (2.1) reproducing the EoS. The temperature- and density-dependent functions $\tilde{g}(T,n)$, $h(T,n)$ defining H are calculated as

$$\tilde{g}(T,n)=\frac{2}{3}\int_0^n\left(\frac{P_{,T}(T,n)}{n^2}-\frac{1}{n}\right)\mathrm{d}n \tag{2.15}$$

$$h(T,n)=\int_0^n\left(\frac{P(T,n)}{n^2}-\frac{TP_{,T}(T,n)}{n^2}\right)\mathrm{d}n \tag{2.16}$$

These relations are obtained by combining the n derivative of the equilibrium condition (2.11) and the temperature derivative of $P(T,n)/T$ in (2.12), resulting in $h_{,n}(T,n)$, i.e. the n derivative of (2.16). Substitution of this $h_{,n}$ into P in (2.12) gives $\tilde{g}_{,n}(T,n)$, i.e. the n derivative of (2.15). The integrations in (2.15) and (2.16) are done according to the boundary conditions $h(T,n=0)=0$ and $\tilde{g}(T,n=0)=0$ or $g(T,n=0)=1/(2m)$, so that the free Hamiltonian of an ideal classical gas is recovered in the limit of vanishing density. It is also assumed that the pressure $P(T,n)$ converges to the pressure $P\sim nT$ of an ideal gas in the limit of vanishing n, so that the integrands in (2.15) and (2.16) are integrable at $n=0$.

In the case of cubic EoSs, the integrals (2.15) and (2.16) can be evaluated in closed form, whereas the integrands defined by the non-cubic EoS in (4.10) do not admit elementary integration but are singularity free and numerically tame, see Section 5. In the case of the van der Waals EoS, the effective Hamiltonian reads $H=g(T,n)p^2+h(T,n)$ with

$$g(T,n)=\frac{1}{2m}(1-bn)^{-2/3},\ h(T,n)=-an,\ P=\frac{nT}{1-bn}-an^2 \tag{2.17}$$

where a and b are positive constants and $n<1/b$. The functions $g(T,n)$ and $h(T,n)$ are calculated from the EoS in (2.17) by way of (2.15) and (2.16). The Hamiltonian (2.4) specified in this way satisfies the equilibrium condition (2.11), and the EoS in (2.12) reproduces the van der Waals EoS in (2.17) as well as the caloric EoS $u(T,n)=3nT/2-an^2$, cf. (2.8).

The effective Hamiltonian of the SRK EoS is analogously defined by

$$g(T,n)=\frac{1}{2m}(1-bn)^{-2/3}(1+bn)^{-2a'(T)/(3b)}$$

$$h(T,n)=\left(Ta'(T)-a(T)\right)\frac{1}{b}\log(1+bn)$$

$$P=\frac{nT}{1-bn}-\frac{a(T)n^2}{1+bn} \tag{2.18}$$

Where $a(T)$ is an empirical temperature dependent factor in the indicated EoS [4]. The prime denotes a temperature derivative.

In the case of the PR EoS, the effective Hamiltonian (2.4) and the EoS are specified by

$$g(T,n)=\frac{1}{2m}(1-bn)^{-2/3}\left(\frac{1+bn\Big/\left(\sqrt{2}-1\right)}{1-bn\Big/\left(\sqrt{2}+1\right)}\right)^{-a'(T)/\left(3\sqrt{2}b\right)}$$

$$h(T,n)=\left(Ta'(T)-a(T)\right)\frac{1}{2\sqrt{2}b}\log\frac{1+bn\Big/\left(\sqrt{2}-1\right)}{1-bn\Big/\left(\sqrt{2}+1\right)}$$

$$P=\frac{nT}{1-bn}-\frac{a(T)n^2}{1+2bn-b^2n^2} \tag{2.19}$$

Here, $a(T)$ is again a temperature dependent empirical factor [4,5]. These equations of state will be further discussed in Section 4.2.

3. Equilibrium condition for the effective Hamiltonian

We consider a partition function of the form

$$\xi=\frac{1}{V}\log Z=\frac{4\pi\sigma}{(2\pi)^3}\int_0^\infty f(-\alpha-\beta H(p;T,n))p^2\mathrm{d}p \tag{3.1}$$

where $f(x)$ and the effective Hamiltonian $H(p;T,n)$ are arbitrary functions. Otherwise, the notation is the same as indicated after in (2.1). The particle density $n=N/V$ and the internal energy density $u=U/V$ admit the integral representations stated in (2.2) and (2.3), with spectral density

$$\mathrm{d}\rho(p)=\frac{4\pi\sigma}{(2\pi)^3}f'(-\alpha-\beta H(p;T,n))p^2\mathrm{d}p \tag{3.2}$$

The prime denotes the derivative of $f(x)$. In the classical case, $f(x)=\mathrm{e}^x$ as in (2.1), and effective fermionic/bosonic quantum distributions are defined by the partition function and spectral density

$$\xi=\frac{\log Z_{\mathrm{F,B}}}{V}=\pm\frac{4\pi\sigma}{(2\pi)^3}\int_0^\infty\log\left(1\pm\mathrm{e}^{-\alpha-\beta H(p;T,n)}\right)p^2\mathrm{d}p \tag{3.3}$$

$$\mathrm{d}\rho_{\mathrm{F,B}}(p)=\frac{4\pi\sigma}{(2\pi)^3}\frac{p^2\mathrm{d}p}{\mathrm{e}^{\alpha+\beta H(p;T,n)}\pm1} \tag{3.4}$$

so that $f_{\mathrm{F,B}}(x)=\pm\log(1\pm\mathrm{e}^x)$. The effective Hamiltonian $H(p;T,n)$ depends on the momentum variable, temperature and particle density.

Eq. (2.2) with spectral density $\mathrm{d}\rho$ in (3.2) can be solved for the fugacity parameter, $\alpha=\alpha(T,n)$. This $\alpha(T,n)$ is then substituted into the spectral density (3.2), the internal energy density (2.3) and the partition function (3.1). Having eliminated the fugacity parameter in this way, we obtain the internal energy density $u=u(T,n)$ and the partition function $\xi=\xi(T,n)$ in (T,n) parametrization. Equation $u=u(T,n)$ can be solved for the temperature variable, $T=\widehat{T}(u,n)$, with derivatives $\widehat{T}_{,u}=1/u_{,T}$ and $\widehat{T}_{,n}=-u_{,n}/u_{,T}$.

We will use (u,n) parametrizations (denoted by a hat) of the fugacity parameter and the partition function,

$$\alpha=\widehat{\alpha}(u,n)=\alpha\left(\widehat{T}(u,n),n\right),\ \xi=\widehat{\xi}(u,n)=\xi\left(\widehat{T}(u,n),n\right) \tag{3.5}$$

which admit the derivatives

$$\widehat{\alpha}_{,u}=\frac{\alpha_{,T}}{u_{,T}},\ \widehat{\alpha}_{,n}=\alpha_{,n}-\alpha_{,T}\frac{u_{,n}}{u_{,T}},\ \widehat{\xi}_{,u}=\frac{\xi_{,T}}{u_{,T}},\ \widehat{\xi}_{,n}=\xi_{,n}-\xi_{,T}\frac{u_{,n}}{u_{,T}} \tag{3.6}$$

expressed in (T,n) parametrization.

The entropy density $s=S(T,N,V)/V$ is assembled from the particle density n, internal energy density u and partition function $\xi=\log Z/V$,

$$s(T,n)=\xi(T,n)+\alpha(T,n)n+u(T,n)/T \tag{3.7}$$

In (u,n) parametrization, this reads

$$s=\widehat{s}(u,n)=s\left(\widehat{T}(u,n),n\right)=\widehat{\xi}(u,n)+\widehat{\alpha}(u,n)n+u\Big/\widehat{T}(u,n) \tag{3.8}$$

with derivatives

$$\widehat{s}_{,u}=\frac{1}{u_{,T}}\left(\xi_{,T}-\frac{u}{T^2}+\alpha_{,T}n\right)+\frac{1}{T} \tag{3.9}$$

$$\widehat{s}_{,n}=\xi_{,n}+\alpha+\left(\alpha_{,n}-\alpha_{,T}\frac{u_{,n}}{u_{,T}}\right)n-\left(\xi_{,T}-\frac{u}{T^2}\right)\frac{u_{,n}}{u_{,T}} \tag{3.10}$$

Since $S(U,N,V)=V\widehat{s}(u,n)$,

$$S_{,U}=\widehat{s}_{,u},\quad S_{,N}=\widehat{s}_{,n},\quad S_{,V}=-\widehat{s}_{,n}n-\widehat{s}_{,u}u+\widehat{s} \tag{3.11}$$

In an equilibrium system, the contact variables are defined by the entropy derivatives $S_{,U}=1/T$, $S_{,V}=P/T$, $S_{,N}=-\mu/T$. The first of these equations thus requires the equilibrium condition, cf. (3.9),

$$\xi_{,T}-\frac{u}{T^2}+\alpha_{,T}n=0 \tag{3.12}$$

By making use of (3.9)–(3.12), we find the entropy derivatives $S_{,N}=\xi_{,n}+\alpha+\alpha_{,n}n$ and $S_{,V}=\xi-\xi_{,n}n-\alpha_{,n}n^2$, which define the pressure (thermal EoS) and the chemical potential,

$$P=T\left(\xi-\xi_{,n}n-\alpha_{,n}n^2\right),\quad \mu=-T\left(\xi_{,n}+\alpha+\alpha_{,n}n\right) \tag{3.13}$$

Eqs. (2.11) and (2.13), which are based on the classical spectral density (2.1) and Hamiltonian (2.4), make these identities more explicit. (In this classical case, $\alpha(T,n)$ and $u(T,n)$ can be calculated in closed form, cf. (2.7) and (2.8), and $\xi(T,n)=n$.)

The isothermal compressibility and the isobaric expansion coefficient are obtained by solving the thermal EoS in (3.13) for the density variable, $n=\widehat{n}(P,T)$:

$$\kappa_T=-\frac{V_{,P}}{V}=\frac{\widehat{n}_{,P}}{\widehat{n}}=\frac{1}{nP_{,n}},\quad \alpha_{\mathrm{exp}}=\frac{V_{,T}}{V}=-\frac{\widehat{n}_{,T}}{\widehat{n}}=\frac{P_{,T}}{nP_{,n}} \tag{3.14}$$

The isochoric/isobaric heat capacities are calculated via $C_V=Vu_{,T}$, $C_P=C_V+VT\alpha_{\mathrm{exp}}^2/\kappa_T$ and the adiabatic compressibility by way of $\kappa_S=\kappa_TC_V/C_P$, which are general equilibrium identities.

4. A non-cubic multi-parameter equation of state

4.1. Adapting cubic EoSs to high-pressure data sets

For the proposed fluid EoS, we use the general ansatz

$$P=g(n,T)-f(n,T)A,\quad A(n,T)=\frac{a(T)}{1+c(T)n+d(T)n^2} \tag{4.1}$$

where $g(n,T)$ and $f(n,T)$ are functions of temperature and molar density n defining the repulsive and attractive terms, respectively. The factor $A(n,T)$ is modeled after the attractive term in the PR EoS, cf. (2.19). The functions $g(n,T)$, $f(n,T)$ and amplitudes $a(T)$, $c(T)$, $d(T)$ will be specified subsequently, and their T dependence will occasionally be suppressed. The critical point is denoted by (P_c,n_c,T_c). The EoS (4.1) is supposed to satisfy the conditions $P_{,n}(n,T)=0$ and $P_{,n,n}(n,T)=0$ at the critical point, which is the inflection point of the T_c isotherm. The resulting three equations

$$\begin{aligned}&P=g-fA,\quad g_{,n}-f_{,n}A-fA_{,n}=0,\\&g_{,n,n}-f_{,n,n}A-2f_{,n}A_{,n}-fA_{,n,n}=0\end{aligned} \tag{4.2}$$

taken at (P_c,n_c,T_c) can unambiguously be solved for the parameters $(a(T_c),c(T_c),d(T_c))$ in (4.1). The first step is to successively solve (4.2) for A, $A_{,n}$ and $A_{,n,n}$:

$$A=\frac{g-P}{f},\quad A_{,n}=\frac{g_{,n}}{f}-f_{,n}\frac{g-P}{f^2}$$

$$A_{,n,n}=\frac{1}{f}\left[g_{,n,n}-f_{,n,n}\frac{g-P}{f}-2f_{,n}\left(\frac{g_{,n}}{f}-f_{,n}\frac{g-P}{f^2}\right)\right] \tag{4.3}$$

Then we calculate the first and second n derivatives of the factor $A(n,T)$ in (4.1) and solve these three equations for (a,c,d), obtaining

$$a=\frac{2A^3}{2A^2+2AA_{,n}n+2A_{,n}^2n^2-AA_{,n,n}n^2}$$

$$c=-\frac{2\left(AA_{,n}+2A_{,n}^2n-AA_{,n,n}n\right)}{2A^2+2AA_{,n}n+2A_{,n}^2n^2-AA_{,n,n}n^2}$$

$$d=-\frac{2A_{,n}^2-AA_{,n,n}}{2A^2+2AA_{,n}n+2A_{,n}^2n^2-AA_{,n,n}n^2} \tag{4.4}$$

taken at the critical point (P_c,n_c,T_c). The third step is to substitute the derivatives (4.3), also taken at (P_c,n_c,T_c), into (4.4). In this way, the coefficients $(a(T_c),c(T_c),d(T_c))$ can be expressed in terms of P and $g(n,T)$, $f(n,T)$ and their first and second n derivatives at the critical point (P_c,n_c,T_c).

We specialize the functions $g(n,T)$ and $f(n,T)$ in (4.1) as

$$g(n,T)=nT\left(1+\left(\frac{n}{b}\right)^{\lambda/\eta}\right)^{\eta},\quad f(n,T)=n^{\alpha(T)} \tag{4.5}$$

where $\alpha(T)$ is a temperature dependent exponent. The exponents λ, η and amplitude b are constants independent of temperature. The EoS (4.1) then reads

$$P=nT\left(1+\left(\frac{n}{b}\right)^{\lambda/\eta}\right)^{\eta}-\frac{n^{\alpha(T)}a(T)}{1+c(T)n+d(T)n^2} \tag{4.6}$$

The cubic equations of state in (2.17)–(2.19) are special cases thereof, cf. Section 4.2.

Introducing the rescaled quantities $\widehat{b}=b/n_c$ and

$$\widehat{A}=\frac{n_c^{\alpha_c-1}}{T_c}A(P_c,n_c,T_c),\ \widehat{A}_{,n}=\frac{n_c^{\alpha_c}}{T_c}A_{,n},\ \widehat{A}_{,n,n}=\frac{n_c^{\alpha_c+1}}{T_c}A_{,n,n} \tag{4.7}$$

where $\alpha_c:=\alpha(T_c)$, we obtain, by making use of (4.3) and (4.5) taken at (P_c,n_c,T),

$$\widehat{A}=\left(1+\widehat{b}^{-\lambda/\eta}\right)^{\eta}-Z_c$$

$$\widehat{A}_{,n}=\alpha_cZ_c+\left(1+\widehat{b}^{-\lambda/\eta}\right)^{\eta-1}\left[1-\alpha_c+\widehat{b}^{-\lambda/\eta}(1-\alpha_c+\lambda)\right]$$

$$\begin{aligned}\widehat{A}_{,n,n}=&-Z_c\alpha_c(1+\alpha_c)+\left(1+\widehat{b}^{-\lambda/\eta}\right)^{\eta-2}\Big[(\alpha_c-1)\alpha_c\\&+\widehat{b}^{-2\lambda/\eta}(\lambda-\alpha_c)(\lambda-\alpha_c+1)+\widehat{b}^{-\lambda/\eta}\Big(2\alpha_c^2-2\alpha_c-2\alpha_c\lambda\\&+\lambda^2\Big/\eta+\lambda\Big)\Big]\end{aligned} \tag{4.8}$$

Here, the critical compressibility factor is denoted by $Z_c=P_c/(n_cT_c)$. A rescaling of the parameters in (4.4) gives

$$\widehat{a}=\frac{n_c^{\alpha_c-1}}{T_c}a(T_c)=\frac{2\widehat{A}^3}{2\widehat{A}^2+2\widehat{A}\widehat{A}_{,n}+2\widehat{A}_{,n}^2-\widehat{A}\widehat{A}_{,n,n}}$$

$$\widehat{c}=n_cc(T_c)=-\frac{2\left(\widehat{A}\widehat{A}_{,n}+2\widehat{A}_{,n}^2-\widehat{A}\widehat{A}_{,n,n}\right)}{2\widehat{A}^2+2\widehat{A}\widehat{A}_{,n}+2\widehat{A}_{,n}^2-\widehat{A}\widehat{A}_{,n,n}}$$

$$\widehat{d}=n_c^2d(T_c)=\frac{2\widehat{A}_{,n}^2-\widehat{A}\widehat{A}_{,n,n}}{2\widehat{A}^2+2\widehat{A}\widehat{A}_{,n}+2\widehat{A}_{,n}^2-\widehat{A}\widehat{A}_{,n,n}} \tag{4.9}$$

with $\widehat{A}$ and its derivatives listed in (4.8) substituted.

It remains to restore the gas constant R in the compressibility factor, $Z_c=P_cV_c/(RT_c)$, where $V_c=1/n_c$ denotes the critical molar volume, so that the parameters in (4.8) and (4.9) are dimensionless constants (denoted by a hat). $n[\mathrm{mol/cm^3}]=N_A/V$ is the molar density, $R=N_Ak_B=8.3145\,\mathrm{J/(K\,mol)}$, and MPa units (that is $\mathrm{J/cm^3}$) are used for pressure.

By introducing reduced quantities, $T_r=T/T_c$, $n_r=n/n_c$, the EoS (4.6) can be written as

$$P(n,T)=Rn_cT_c\left[n_rT_r\left(1+\left(\frac{n_r}{\widehat{b}}\right)^{\lambda/\eta}\right)^{\eta}-\frac{n_r^{\alpha(T)}\sigma(T)}{1+\rho(T)n_r+\chi(T)n_r^2}\right] \tag{4.10}$$

At the critical temperature, the constants $\sigma(T_c)=\widehat{a}$, $\rho(T_c)=\widehat{c}$ and $\chi(T_c)=\widehat{d}$ have been calculated in (4.8) and (4.9). The temperature-dependent dimensionless functions $\sigma(T)=(n_c^{\alpha(T)-1}/T_c)a(T)$, $\rho(T)=n_cc(T)$, $\chi(T)=n_c^2d(T)$, cf. (4.1), and the exponent $\alpha(T)$ are otherwise arbitrary. The stated values of $\sigma(T)$, $\rho(T)$, $\chi(T)$ at T_c are defined by the three conditions $P_c=P(n_c,T_c)$, $P_{,n}(n_c,T_c)=0$ and $P_{,n,n}(n_c,T_c)=0$, see after (4.1). The exponents λ, η and the dimensionless amplitude $\widehat{b}$ are temperature-independent fitting parameters, to be determined from the T_c isotherm.

When performing isothermal fits in Section 4.3, we will use a positive amplitude $\widehat{b}$ as well as positive exponents λ, η, so that the repulsive term of the EoS (4.10) is non-singular, in contrast to cubic

EoSs, cf. Section 4.2. The EoS (4.10) can accurately reproduce the isotherms in the high-pressure/high-density regime, which admit nearly straight power-law slopes in log-log plots, cf. Section 4.3. Finally, since the exponents λ, η and $\alpha(T)$ are non-integer, obtained from least-squares fits, the virial expansion of the EoS (4.10) contains non-integer powers of the reduced density n_r, in contrast to cubic EoSs [33–35].

4.2. Cubic equations as special cases: Peng-Robinson and Soave-Redlich-Kwong EoS

Cubic equations of state can be obtained from the EoS (4.10) by specifying the parameters as $\alpha = 2$, $\lambda = \eta = -1$ and $\widehat{b} = -1/\widehat{p}$ with $\widehat{p} > 0$. We then find, via (4.8) and (4.9),

$$\widehat{a} = (1 + (\widehat{p} - 1)Z_\mathrm{c})^3 \Big/ Z_\mathrm{c} \tag{4.11}$$

$$\widehat{c} = 1/Z_\mathrm{c} + \widehat{p} - 3 \tag{4.12}$$

$$\widehat{d} = 3\widehat{p} - 2\widehat{p}^2 - \widehat{p}/Z_\mathrm{c} - (\widehat{p} - 1)^3 Z_\mathrm{c} \tag{4.13}$$

The amplitudes $\rho(T)$ and $\chi(T)$ in the EoS (4.10) are assumed to be constants, $\rho(T) = \widehat{c}$, $\chi(T) = \widehat{d}$ (see after (4.10)), and the temperature-dependent third amplitude can be written as $\sigma(T) = \widehat{a}\widehat{\sigma}(T)$, with $\widehat{\sigma}(T_\mathrm{c}) = 1$. The EoS (4.10) then simplifies to the cubic equation

$$P(n,T) = Rn_\mathrm{c}T_\mathrm{c}\left(\frac{n_\mathrm{r}T_\mathrm{r}}{1-\widehat{p}n_\mathrm{r}} - \frac{n_\mathrm{r}^2\widehat{a}\widehat{\sigma}(T)}{1+\widehat{c}n_\mathrm{r}+\widehat{d}n_\mathrm{r}^2}\right) \tag{4.14}$$

In the case of the PR and SRK equations, $\widehat{p}$ and Z_c are specified as universal constants in (4.11)–(4.13). The Patel-Teja and Trebble-Bishnoi generalizations [36–42] of the PR EoS are also special cases of the cubic EoS (4.14). The repulsive term in (4.14) always leads to a singularity at $n_\mathrm{r} = 1/\widehat{p}$, irrespective of whether $\widehat{p}$ is treated as universal constant or fit parameter.

In Section 4.3, quantitative comparisons of the PR EoS with the non-cubic EoS (4.10) will be performed, by using pressure isotherms of classical and quantum fluids. In the PR EoS, the parameters $\widehat{p}$ and Z_c in (4.11)–(4.13) are specified as

$$\widehat{p} = \frac{1}{3}\left(\frac{2}{r} - 1 - r\right), \quad Z_\mathrm{c} = \frac{3r}{2 + 8r - r^2}, \quad r = \left(6\sqrt{2} - 8\right)^{1/3} \tag{4.15}$$

That is, $\widehat{p} = 0.253077$, $Z_\mathrm{c} = 0.307401$ and thus, cf. (4.11)–(4.13), $\widehat{a} = 1.48742$, $\widehat{c} = 0.506153$ and $\widehat{d} = -0.0640478$. This rather peculiar choice of parameters can be motivated as follows. The denominator of the attractive term in the EoS (4.14) can be factorized as $1 + \widehat{c}n_\mathrm{r} + \widehat{d}n_\mathrm{r}^2 = (1 + \widehat{\alpha}\widehat{p}n_\mathrm{r})(1 - \widehat{\beta}\widehat{p}n_\mathrm{r})$, so that $\widehat{c} = (\widehat{\alpha} - \widehat{\beta})\widehat{p}$ and $\widehat{d} = -\widehat{\alpha}\widehat{\beta}\widehat{p}^2$, to be substituted into Eqs. (4.12) and (4.13). We then solve Eq. (4.12) for Z_c,

$$Z_\mathrm{c} = \frac{1}{\left(\widehat{\alpha} - \widehat{\beta}\right)\widehat{p} - \widehat{p} + 3} \tag{4.16}$$

and substitute this into (4.13) to arrive at a cubic equation for $\widehat{p}$,

$$1 - 3\widehat{p} + 3\left(-\widehat{\alpha} + \widehat{\beta} + \widehat{\alpha}\widehat{\beta}\right)\widehat{p}^2 + \left(-\widehat{\alpha}^2 + \widehat{\alpha}\widehat{\beta} + \widehat{\alpha}^2\widehat{\beta} - \widehat{\beta}^2 - \widehat{\alpha}\widehat{\beta}^2\right)\widehat{p}^3 = 0 \tag{4.17}$$

The numerical values for $\widehat{p}$ and Z_c in (4.15) are obtained from (4.16) and (4.17) with the parameter choice $\widehat{\alpha} = 1/(\sqrt{2}-1)$ and $\widehat{\beta} = 1/(\sqrt{2}+1)$; $\widehat{p}$ stated in (4.15) is the only real solution of (4.17). By the way, the van der Waals equation in (2.17) corresponds to the parameter choice $\widehat{\alpha} = \widehat{\beta} = 0$ in (4.16) and (4.17), so that $\widehat{p} = 1/3$, $Z_\mathrm{c} = 3/8$, $\widehat{c} = \widehat{d} = 0$, $\widehat{a} = 9/8$, cf. (4.11)–(4.13).

In the case of the SRK equation, it is assumed in (4.11)–(4.13) that $Z_\mathrm{c} = 1/3$, so that $\widehat{c} = \widehat{p}$, and furthermore that $\widehat{d} = 0$, so that (4.13) gives a cubic equation for $\widehat{p}$ which admits the unique real solution $\widehat{p} = 2^{1/3} - 1 = 0.259921$, and accordingly $\widehat{a} = 1.28244$, cf. (4.11). In (4.16) and (4.17), this EoS corresponds to the parameter choice $\widehat{\alpha} = 1$ and $\widehat{\beta} = 0$.

The temperature dependent factor $\widehat{\sigma}(T)$ ('alpha function') in the cubic EoS (4.14) has to be empirically determined. (In the van der Waals equation, $\widehat{\sigma}(T) = 1$ by definition.) In the case of the PR and SRK equations, a frequently used analytic shape is $\widehat{\sigma}(T) = (1 + \Omega(\omega)(1 - \sqrt{T_\mathrm{r}}))^2$, where Ω depends on the acentric factor ω of the fluid [4,43]. Recent estimates of Ω for the PR and SRK equations, regressed from 1721 compounds [22], read

$$\Omega_\mathrm{PR}(\omega) = 0.3919 + 1.4996\omega - 0.2721\omega^2 + 0.1063\omega^3 \tag{4.18}$$

$$\Omega_\mathrm{SRK}(\omega) = 0.4810 + 1.5963\omega - 0.2963\omega^2 + 0.1223\omega^3 \tag{4.19}$$

A large number of other analytic functions $\widehat{\sigma}(T)$ have been suggested for cubic equations of type (4.14), see Table 1 of Ref. [5], usually involving the first few terms of a power series in $1 - \sqrt{T_\mathrm{r}}$ or $1 - T_\mathrm{r}$, cf., e.g., Refs. [7–21].

4.3. Testing equations of state with pressure isotherms of classical and quantum fluids

Figs. 1–8 show least-squares fits of the non-cubic multi-parameter EoS (4.10) to pressure isotherms of nitrogen, carbon monoxide, methane, carbon dioxide, methanol and water, as well as to the quantum fluids hydrogen and helium. The data sets are taken from Ref. [6] and cover an extended pressure range, up to 1 GPa. Fits are performed to the critical isotherm and to isotherms at super- and subcritical temperatures. The isotherms are depicted in double-logarithmic representation to better identify straight power-law slopes emerging at high density above the critical point. The critical and fitting parameters of the EoS (4.10) are listed in Tables 1–3. Also indicated in Figs. 1–8 are the pressure isotherms (dotted blue curves) of the PR EoS (4.14) (with parameters in (4.15), (4.18) and Table 1) which is known to give slightly better approximations to measured isotherms than the SRK EoS [16,17].

The PR EoS (and, for that matter, also the SRK EoS) satisfies the required conditions $P_{,n}(n_\mathrm{c}, T_\mathrm{c}) = 0$ and $P_{,n,n}(n_\mathrm{c}, T_\mathrm{c}) = 0$ at the critical point, see after (4.1), but the condition $P_\mathrm{c} = P(n_\mathrm{c}, T_\mathrm{c})$ is satisfied only if the assumed value of the compressibility factor, $Z_\mathrm{c} = P_\mathrm{c}/(RT_\mathrm{c}n_\mathrm{c}) = 0.307$, is consistent with the actually measured critical parameters $(P_\mathrm{c}, n_\mathrm{c}, T_\mathrm{c})$, cf. Table 1. In the PR equation, this prescribed Z_c is a universal constant, cf. (4.15). However, $P_\mathrm{c}/(RT_\mathrm{c}n_\mathrm{c})$ is about 0.22 for methanol and 0.23 for water and as low as 0.117 for hydrogen fluoride, which means that the critical isotherm defined by the PR equation is off the mark at the critical point, see Figs. 5 and 6. (The critical isotherm is independent of the choice of the empirical alpha function $\widehat{\sigma}(T)$, since $\widehat{\sigma}(T_\mathrm{c}) = 1$ by definition, cf. (4.14) and (4.18).) The measured critical compressibility factor Z_c is usually smaller than 0.3, except for quantum fluids where it is slightly larger [4,43].

According to the cubic EoS (4.14), the maximal reduced density attainable is $n_\mathrm{r}^\mathrm{max} = 1/\widehat{p}$, at which the repulsive term of the EoS

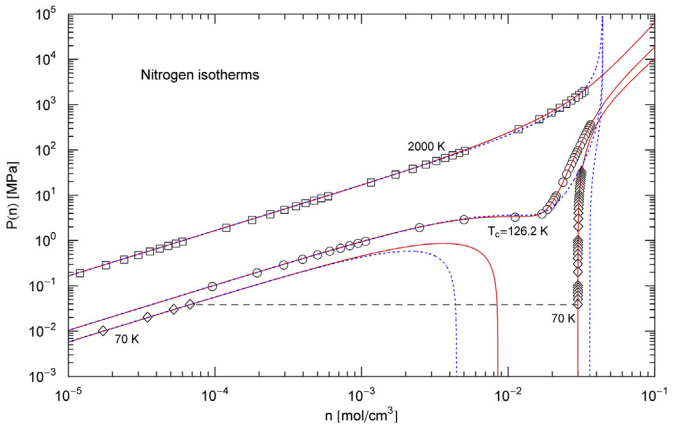

Fig. 1. Nitrogen pressure isotherms. Data points from Ref. [6]; squares/circles/diamonds indicate supercritical/critical/subcritical data points, respectively, at the indicated temperature. The solid red curves depict least-squares fits of the non-cubic multi-parameter EoS (4.10). The fit parameters and determination coefficients are recorded in Tables 2 and 3. The dashed black line connects the saturation points on the 70 K subcritical isotherm, crossing the vapor/liquid coexistence region. The dotted blue curves show the PR approximation defined in (4.14), (4.15) and (4.18), with critical temperature, critical density and acentric factor listed in Table 1. The PR EoS predicts a singularity of the pressure isotherms at the limit density $n_c/\widehat{p} = 0.044\,\mathrm{mol/\,cm^3}$, cf. (4.15), in contrast to EoS (4.10).

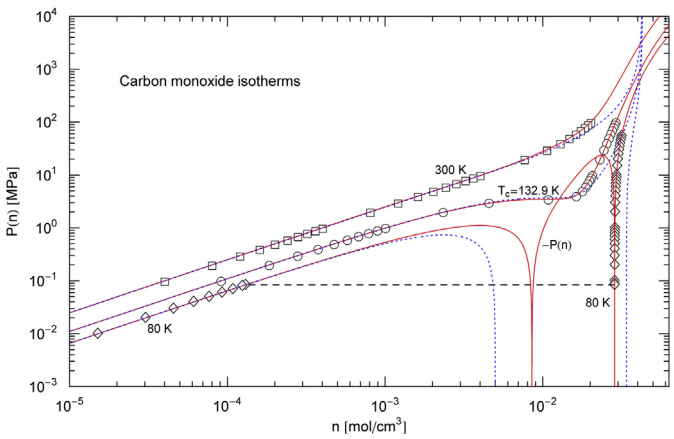

Fig. 2. Carbon monoxide pressure isotherms. Data points from Ref. [6]. The log-log plots show the critical isotherm at $T_c = 132.9$ K as well as sub- and supercritical isotherms at 80 K and 300 K (solid red curves). The least-squares fits are performed with the non-cubic EoS (4.10), the fitting parameters are listed in Tables 2 and 3, and the critical parameters in Table 1. The negative component of the 80 K subcritical isotherm, where the local minimum of the Maxwell loop is located, is depicted as $-P(n)$ in this log-log representation; the preceding local maximum is also clearly visible. Subcritical pressure isotherms of EoS (4.10) have two local extrema defining a single loop. The dotted blue curves depict the PR approximation of the isotherms, based on Eqs. (4.14), (4.15) and (4.18).

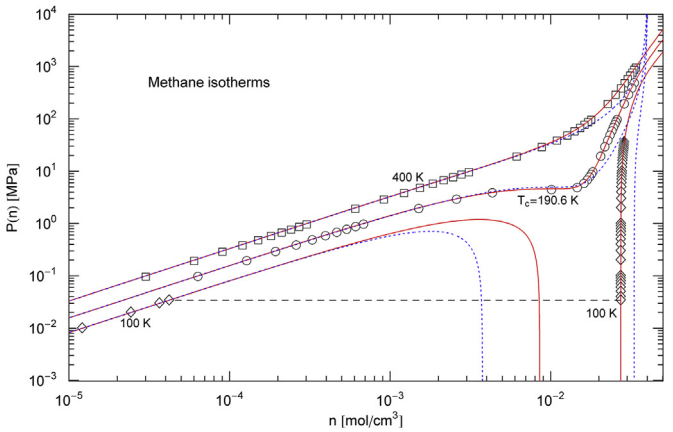

Fig. 3. Methane pressure isotherms. Data points from Ref. [6]. Depicted are the critical isotherm at 190.6 K and sub- and supercritical isotherms at 100 K and 400 K (solid red curves). The fits are performed with EoS (4.10). The ascent of the 100 K isotherm in the liquid phase is extremely steep and requires fit parameters accurate to several decimal digits as listed in Tables 2 and 3. The dotted curves indicate the PR approximation of the isotherms, which gives good fits of the three data sets only below the critical density of 0.010 mol/cm^3. The 100 K PR isotherm (dotted, blue) in the liquid phase and the critical PR isotherm deviate noticeably from the high-density data points.

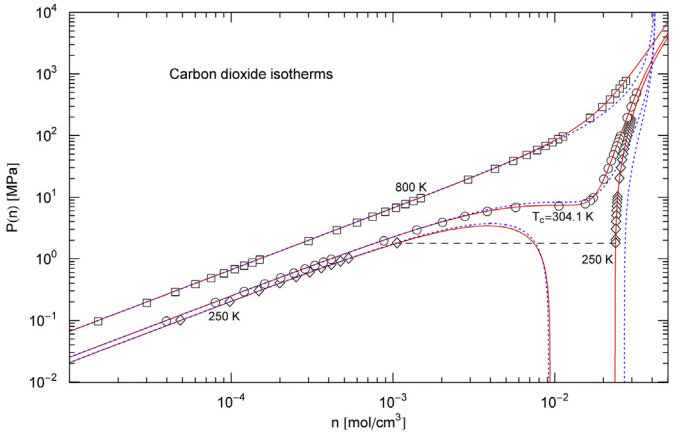

Fig. 4. Carbon dioxide pressure isotherms. Data points from Ref. [6]. Depicted are the critical isotherm at 304.1 K as well as sub- and supercritical isotherms at 250 K and 800 K (solid red curves). The dashed black line connects the saturation points on the subcritical isotherm. The least-squares fits are performed with the multi-parameter EoS (4.10), the fitting parameters are recorded in Tables 2 and 3, the critical parameters in Table 1. The dotted blue curves show the PR isotherms, which fail to reproduce the data sets above the critical density of 0.011 mol/cm^3, in particular the nearly straight power-law slope of the critical isotherm, in contrast to the isotherms of EoS (4.10) (solid red curves).

becomes singular and the pressure diverges (as illustrated by the dotted curves depicting PR isotherms in Figs. 1–8). The parameter $\widehat{p}$ is a universal constant in the PR and SRK equations, cf. (4.15). Instead of assuming universal prescribed values for Z_c and $\widehat{p}$, one can use the measured value of $Z_c = P_c/(RT_cn_c)$ in Eqs. (4.11) and (4.13), so that the general cubic EoS in (4.14) is satisfied at the critical point, $P_c = P(n_c, T_c)$, and one can try to specify the parameter $\widehat{p}$ by fitting the critical isotherm (which becomes singular at $n_r = 1/\widehat{p}$) to a data set. However, the actual problem with cubic equations is the lack of any indication of a singularity in experimental pressure isotherms. If one uses double-logarithmic plots for the isothermal data points, as done in Figs. 1–8, one finds a nearly straight power-law increase of the pressure at high density, rather than a sudden upward bend of the isotherms indicating a singularity. The power-law slope of the critical isotherms is particularly pronounced. Therefore, in the absence of a singularity indicated by the data points, and irrespective of whether $\widehat{p}$ is a prescribed or fitting parameter (since this parameter defines a singularity in the cubic EoS (4.14) in any case), cubic EoSs tend to be inaccurate at high pressure, as they predict a singularity instead of the measured power-law increase of the pressure isotherms apparent in log-log plots. In contrast, the multi-parameter EoS (4.10) reproduces the power-law slope emerging in the isothermal data sets above the

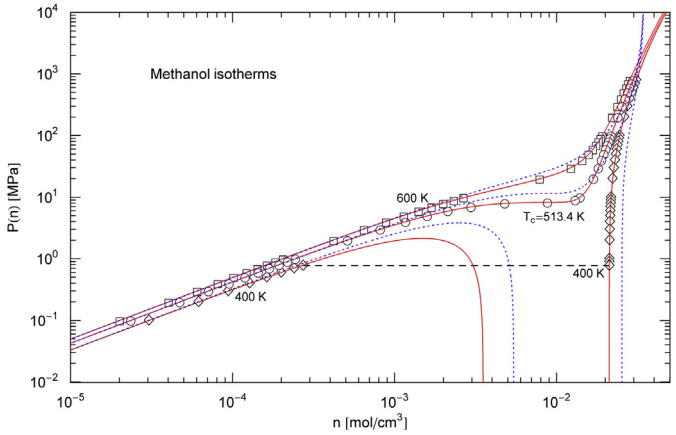

Fig. 5. Methanol pressure isotherms. Data points from Ref. [6]. Depicted are the critical isotherm at $T_c = 513.4$ K and sub- and supercritical isotherms at 400 K and 600 K (solid red curves). The least-squares fits are performed with the non-cubic multi-parameter EoS (4.10), the fitting parameters are listed in Tables 2 and 3. In contrast to Figs. 1–4, the PR approximation (dotted, blue) of the critical isotherm is inaccurate at the critical point (P_c, n_c, T_c), $n_c = 8.8 \times 10^{-3}$mol/cm^3, since the critical compressibility factor Z_c of methanol (see Table 1) substantially deviates from the universal Z_c assumed in the PR equation, cf. (4.15).

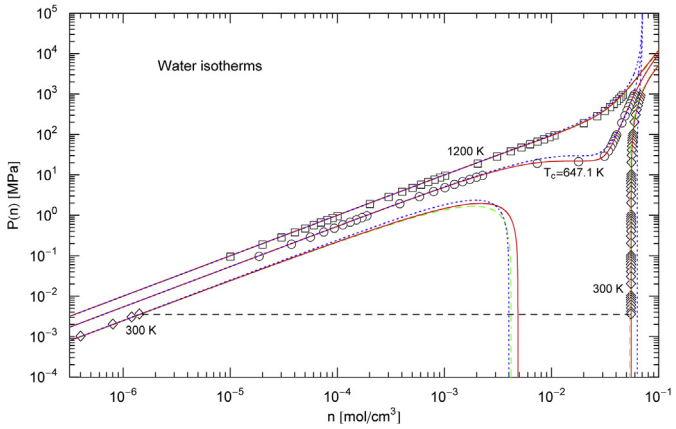

Fig. 6. Water pressure isotherms. Data points from Ref. [6]. Depicted are the critical isotherm at 647.1 K and sub- and supercritical isotherms at 300 K and 1200 K (solid red curves). The fits are performed with the EoS (4.10), the fitting parameters are listed in Tables 2 and 3, the critical parameters in Table 1. The dashed green curves, which almost perfectly coincide with the 1200 K isotherm and the subcritical 300 K isotherm in the liquid phase (solid red curves) are also based on EoS (4.10). In this case, the amplitudes $\sigma(T)$, $\rho(T)$, $\chi(T)$ and exponent $\alpha(T)$ in the attractive term of EoS (4.10) are treated as analytic functions of temperature rather than as fit parameters, cf. Section 4.4, Fig. 9 and Table 4. At the critical temperature, these functions coincide with the parameters $\sigma(T_c)$, $\rho(T_c)$, $\chi(T_c)$ and $\alpha(T_c)$ listed in Table 2, so that the critical isotherm (solid red curve) is exactly reproduced. The dotted blue curves show the PR isotherms, based on Eqs. (4.14), (4.15) and (4.18). As in the case of methanol, cf. Fig. 5, the critical compressibility factor of water $Z_c = 0.23$ deviates from the universal $Z_c = 0.31$ assumed in the PR EoS, cf. (4.15) and Table 1, which is the reason for the inaccurate approximation (dotted, blue) of the critical isotherm in the vicinity of the critical density $n_c = 1.8 \times 10^{-2}$mol/cm^3.

critical density and even the low-temperature isotherms of quantum fluids, see Figs. 7 and 8, and gives a definite prediction of the isotherms above the pressure limit of 1 GPa of the data sets.

4.4. Temperature evolution of pressure isotherms

To obtain the temperature parametrization of EoS (4.10) requires

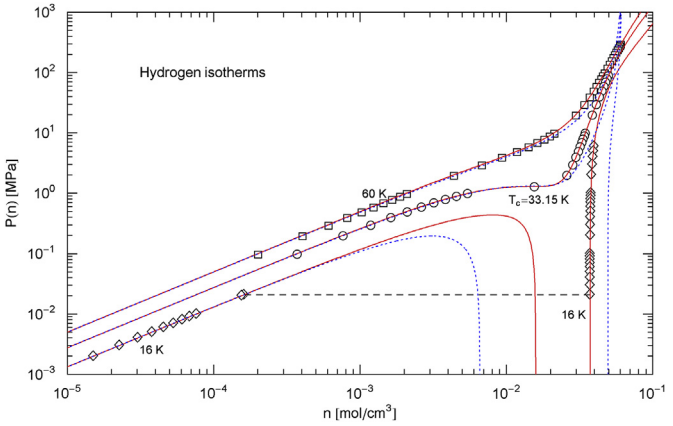

Fig. 7. Hydrogen pressure isotherms. Data points from Ref. [6]. Depicted are the critical isotherm at $T_c = 33.15$ K as well as sub- and supercritical isotherms at 16 K and 60 K (solid red curves). The least-squares fits are performed with the EoS (4.10). Even though hydrogen is a quantum fluid at low temperature, the classical multi-parameter EoS (4.10) gives accurate fits to the data sets. The fit parameters recorded in Tables 2 and 3 are also similar to those of the classical gases/liquids in Figs. 1–6. The dotted blue curves show the PR approximation, which deviates from the data points above the critical density $n_c = 1.55 \times 10^{-2}$mol/cm^3; especially the nearly straight power-law slope of the critical isotherm is not reproduced by the PR EoS.

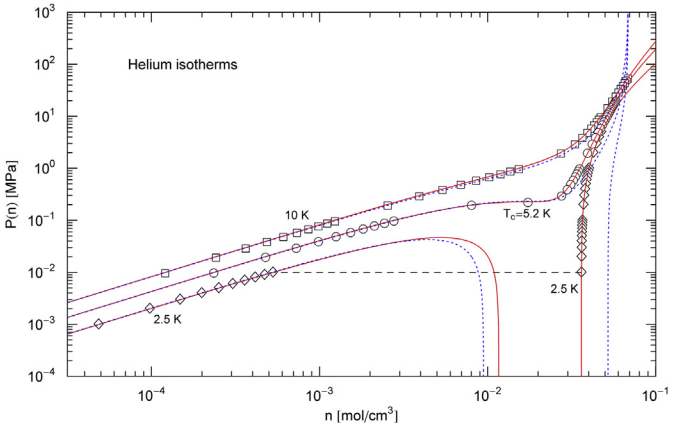

Fig. 8. Helium pressure isotherms. Data points from Ref. [6]. Depicted are the critical isotherm at $T_c = 5.2$ K and sub- and supercritical isotherms at 2.5 K and 10 K (solid red curves). The least-squares fits are performed with the non-cubic EoS (4.10), the fitting parameters are listed in Tables 2 and 3, the critical parameters in Table 1. As in the case of hydrogen, cf. Fig. 7, the PR approximation (dotted blue curves) fails at high density for this quantum liquid, whereas the isotherms of the multi-parameter EoS (4.10) accurately fit these low-temperature data sets.

Table 1
Critical temperature T_c, particle density n_c and pressure P_c of the fluids in Figs. 1–8, cf. Ref. [6]. The critical compressibility factor is $Z_c = P_c/(n_c T_c R)$, cf. after (4.9). Also listed is the acentric factor ω used in the alpha function of the PR EoS, cf. (4.14) and (4.18).

	T_c[K]	n_c[mol/cm^3]	P_c[MPa]	Z_c	ω
Nitrogen	126.19	0.011184	3.3958	0.28939	0.0372
Carbon monoxide	132.86	0.010850	3.4982	0.29187	0.050
Methane	190.56	0.010139	4.5992	0.28629	0.01142
Carbon dioxide	304.13	0.010634	7.3773	0.27435	0.22394
Methanol	513.38	0.0087851	8.2158	0.21909	0.5625
Water	647.10	0.017868	22.064	0.22951	0.3443
Hydrogen	33.145	0.015508	1.2964	0.30334	−0.219
Helium	5.1953	0.017399	0.22637	0.30120	−0.382

Table 2
Fitting parameters of the critical pressure isotherms in Figs. 1–8. The EoS used for the least-squares fits reads, cf. (4.10),

$$P(n,T) = Rn_cT_c\left[n_rT_r\left(1+\left(\frac{n_r}{\widehat{b}}\right)^{\lambda/\eta}\right)^{\eta} - \frac{n_r^{\alpha(T)}\sigma(T)}{1+\rho(T)n_r+\chi(T)n_r^2}\right]$$

where $T_r = T/T_c$ and $n_r = n/n_c$ denote the reduced temperature and molar density and R is the gas constant. The amplitude $\widehat{b}$ and exponents λ, η in the repulsive term are constants independent of temperature, applying to all isotherms of a given fluid. The critical isotherm is fitted with T_c in Table 1; the listed fit parameters are $\widehat{b}$, λ, η and the exponent $\alpha(T_c)$ in the attractive term. R^2 is the determination coefficient of the fits as defined in Eq. (1) of Ref. [44]. Also recorded are the critical amplitudes $\sigma(T_c)$, $\rho(T_c)$, $\chi(T_c)$ in the attractive term of the EoS, calculated from the fit parameters and the compressibility factor Z_c, cf. after (4.10) and Table 1.

	$\widehat{b}$	λ	η	$\alpha(T_c)$	$1-R^2$	$\sigma(T_c)$	$-\rho(T_c)$	$\chi(T_c)$
Nitrogen	0.65946	1.9992	1.0064	2.1927	1.1×10^{-4}	1.9235	0.45523	0.091688
Carbon monoxide	0.65789	2.1141	2.1705	2.0146	1.4×10^{-4}	4.8910	0.36728	0.062285
Methane	0.68156	1.9910	0.96812	2.1669	2.0×10^{-4}	1.7517	0.46924	0.095506
Carbon dioxide	0.66190	1.9768	0.97380	2.1563	8.5×10^{-5}	1.8393	0.46680	0.093635
Methanol	0.19854	1.5062	1.2398	2.1968	9.3×10^{-5}	10.994	0.20099	0.032886
Water	0.62168	1.4623	0.62176	2.0228	3.1×10^{-5}	1.5360	0.36242	0.073629
Hydrogen	0.79528	1.8611	0.77971	2.0638	1.5×10^{-4}	1.1398	0.50767	0.11286
Helium	0.66533	1.8384	0.89045	2.1840	1.6×10^{-4}	1.7358	0.42716	0.092404

Table 3
Fit parameters of sub- and supercritical pressure isotherms. The EoS used in the least-squares fits is stated in (4.10), also see the caption to Table 2. The fit parameters at non-critical temperature are the exponent $\alpha(T)$ and the amplitudes $\sigma(T)$, $\rho(T)$, $\chi(T)$ in the attractive term of the EoS. $\rho(T)$ is negative except at high temperature. R^2 is the determination coefficient of the fits. The isotherms corresponding to the lowest/highest temperatures listed are depicted in Figs. 1–8. (The temperature selection is largely based on the availability of data points.)

T[K]	$\alpha(T)$	$\sigma(T)$	$-\rho(T)$	$\chi(T)$	$1-R^2$
Nitrogen					
70	1.8756	1.0184	0.59100	0.11594	6.5×10^{-6}
100	2.0226	1.5932	0.50502	0.099803	1.9×10^{-4}
300	2.8202	4.3128	0.20447	0.054336	4.3×10^{-5}
2000	3.8747	84.367	−1.9556	0.018031	1.3×10^{-5}
Carbon monoxide					
80	1.9292	2.8873	0.44415	0.079420	5.0×10^{-5}
200	2.0632	6.8460	0.36252	0.062283	2.4×10^{-4}
300	2.0596	9.3691	0.40517	0.076878	3.8×10^{-6}
Methane					
100	1.8404	0.85185	0.61430	0.12170	1.0×10^{-6}
400	2.7720	3.4973	0.23282	0.059925	9.9×10^{-6}
Carbon dioxide					
250	1.9897	1.5978	0.50339	0.097161	5.0×10^{-5}
500	2.6109	2.8412	0.30989	0.072803	3.3×10^{-6}
800	3.1190	5.5832	−0.081886	0.028357	4.2×10^{-6}
Methanol					
400	2.0731	8.3901	0.25908	0.040010	1.9×10^{-4}
600	2.2419	12.904	0.17697	0.030092	1.4×10^{-4}
Water					
300	1.5403	0.88641	0.50245	0.092592	1.8×10^{-3}
800	2.3358	1.8339	0.26016	0.068111	2.3×10^{-5}
1000	2.6380	2.2498	0.13313	0.065580	5.9×10^{-6}
1200	2.9669	3.1202	−0.12792	0.069701	5.4×10^{-6}
Hydrogen					
16	1.7655	0.45906	0.72982	0.16941	5.0×10^{-6}
60	2.6368	1.8700	0.30062	0.074979	8.6×10^{-5}
Helium					
2.5	1.8468	0.81117	0.63709	0.15740	2.6×10^{-4}
10	2.5876	3.3314	0.23913	0.053552	3.5×10^{-5}

to specify the temperature dependent exponent $\alpha(T)$ and amplitudes $\sigma(T)$, $\rho(T)$, $\chi(T)$ defining the attractive term of the EoS as analytic functions of temperature. (In Section 4.3, we have treated these functions as temperature dependent fitting parameters.) At temperatures close to T_c, these functions can be represented by power series expansions, $\alpha(T) = \alpha(T_c)[1 + c_1(1-T/T_c) + c_2(1-T/T_c)^2 + \cdots]$, and analogously for the three amplitudes. The critical parameters $\alpha(T_c)$, $\sigma(T_c)$, etc., are taken from Table 2. (An expansion in powers of $1-\sqrt{T/T_c}$, which is more frequently used for the alpha function of the PR equation, cf. Table 1 of Ref. [5], has been found to give poorer fits in this context than the indicated Taylor series.)

The series coefficients $c_{1,2}$ are inferred from polynomial least-squares fits. To this end, one calculates several pressure isotherms of a given compound at temperatures close to critical, as depicted in Figs. 1–8, by treating the temperature dependent exponent and amplitudes as fitting parameters rather than as functions of temperature. In this way, four data sets $(T_i,\alpha(T_i))$, $(T_i,\sigma(T_i))$, $(T_i,\rho(T_i))$, $(T_i,\chi(T_i))$ are obtained as listed in Table 3 for each compound. The above analytic series expansions are then fitted to these data sets to determine the series coefficients $c_{1,2}$ (which are compound dependent). This is done in Fig. 9 for water pressure isotherms; the data points are taken from Table 3, the critical parameters $\alpha(T_c)$, etc., from Table 2. The series coefficients $c_{1,2}$, obtained by linear least-squares regression, cf. Fig. 9, are recorded in Table 4. Once these coefficients are determined, one can substitute the analytic expansions of the exponent $\alpha(T)$ and amplitudes $\sigma(T)$, $\rho(T)$, $\chi(T)$ into the EoS (4.10) to find the temperature parametrization of the EoS in the vicinity of the critical temperature.

The water pressure isotherms parametrized by temperature are depicted in Fig. 6 as dashed green curves, approximating the sub- and supercritical isotherms (red solid curves, calculated by treating the temperature dependent exponent and amplitudes as fitting parameters, cf. Section 4.3) quite well, especially at high pressure. The critical isotherm, which is the starting point of the above series expansions, is exactly reproduced. For water pressure isotherms, the range of applicability of these expansions is at least 300 K − 1200 K (that is roughly $0.5 \le T_r \le 2$, cf. Fig. 9) as suggested by the temperatures of the sub- and supercritical isotherms depicted in Fig. 6.

Higher orders can be included in the above power series expansions (truncated after the second order), although this requires larger data sets $(T_i,\alpha(T_i))$, $(T_i,\sigma(T_i))$, etc. Combined fits including data sets of thermodynamic variables other than pressure can also be performed, by adding the least-squares $\widehat{\chi}^2$ functionals of the first and second temperature derivatives, e.g., $\widehat{\chi}^2(\alpha) + \widehat{\chi}^2(\alpha') + \widehat{\chi}^2(\alpha'')$. The data sets $(T_i,\alpha'(T_i))$, $(T_i,\alpha''(T_i))$ required in the functionals

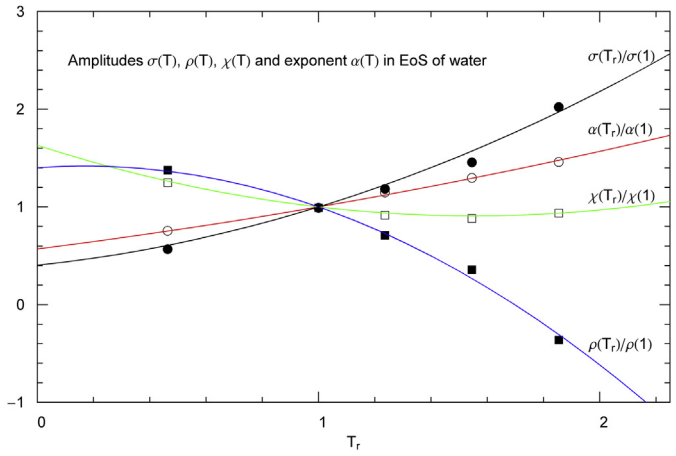

Fig. 9. Temperature variation of the amplitudes $\sigma(T)$, $\rho(T)$, $\chi(T)$ and exponent $\alpha(T)$ in the attractive term of EoS (4.10) applied to water, cf. Section 4.4. Depicted are four least-squares fits based on data points in Table 3 (for sub- and supercritical T). The fit functions are here parametrized by reduced temperature and defined by power series expansions around the critical temperature, e.g., $\sigma(T_r)/\sigma(1) = 1 + c_1(1 - T_r) + c_2(1 - T_r)^2 + \cdots$. The critical parameters $\sigma(1)$, $\rho(1)$, $\chi(1)$, $\alpha(1)$ of water are taken from Table 2 and the fit parameters $c_{1,2}$ are listed in Table 4. Water pressure isotherms obtained by substituting these series expansions into EoS (4.10) are shown in Fig. 6 as dashed green curves.

Table 4
Analytic representation of the exponent $\alpha(T)$ and amplitudes $\sigma(T)$, $\rho(T)$, $\chi(T)$ in EoS (4.10) of water. In the vicinity of the critical temperature, these functions are defined by power series expansions, $\alpha(T) = \alpha(T_c)[1 + c_1(1 - T/T_c) + c_2(1 - T/T_c)^2 + \cdots]$ and analogously for the three amplitudes, cf. Section 4.4. The critical constants $\alpha(T_c)$, etc., are obtained from the critical pressure isotherm of water, cf. Table 2. Listed are the first two expansion coefficients $c_{1,2}$, inferred from the least-squares fits depicted in Fig. 9. The series expansions are applicable in the temperature range 300 K – 1200 K, see Fig. 6.

	$\alpha(T)$	$\sigma(T)$	$\rho(T)$	$\chi(T)$
c_1	−0.49895	−0.88869	1.00867	0.33155
c_2	0.069905	0.29303	−0.60795	0.300095

$\widehat{\chi}^2(\alpha')$ and $\widehat{\chi}^2(\alpha'')$ can be obtained from isothermal least-squares fits of the internal energy and isochoric heat capacity, respectively, which depend on the first and second temperature derivatives of the exponent $\alpha(T)$, cf. Section 5. The same holds true for the amplitudes $\sigma(T)$, $\rho(T)$, $\chi(T)$ and their derivatives.

The asymptotic high-temperature regime $T/T_c >> 1$ of the exponent $\alpha(T)$ and amplitudes $\sigma(T)$, $\rho(T)$, $\chi(T)$ is outside the reach of ascending series expansions. To this end, one will have to use data sets $(T_i,\ \alpha(T_i))$, $(T_i,\ \sigma(T_i))$, etc., obtained from high-temperature isotherms and find analytic expressions, typically composed of power laws and exponentials, which can be used as fit functions.

5. Effective Hamiltonian and internal energy derived from a non-cubic multi-parameter EoS

In Section 2.2, we explained the reconstruction of the effective Hamiltonian $H = g(T,n)p^2 + h(T,n)$ from a general EoS and gave explicit examples for cubic EoSs. Here, we calculate the coefficient functions $h(T,n)$ and $g(T,n) = e^{\tilde{g}(T,n)}/(2m)$ based on the non-cubic EoS (4.10). To this end, we need the temperature derivative of EoS (4.10),

$$P_{,T} = Rn_cT_c\left[\frac{n_r}{T_c}\left(1+\left(\frac{n_r}{\widehat{b}}\right)^{\lambda/\eta}\right)^{\eta} - \frac{n_r^{\alpha}\log n_r}{1+\rho n_r+\chi n_r^2}\sigma\alpha' - \frac{n_r^{\alpha}}{1+\rho n_r+\chi n_r^2}\sigma' + \frac{n_r^{\alpha+1}}{(1+\rho n_r+\chi n_r^2)^2}\sigma\rho' + \frac{n_r^{\alpha+2}}{(1+\rho n_r+\chi n_r^2)^2}\sigma\chi'\right] \tag{5.1}$$

The primes denote derivatives of the amplitudes $\sigma(T)$, $\rho(T)$, $\chi(T)$ and exponent $\alpha(T)$ in (4.10). The coefficient functions defining the effective Hamiltonian read, cf. (2.15) and (2.16),

$$h(T,n) = \frac{1}{n_c}\int_0^{n_r}\left(\frac{P}{n_r^2} - \frac{TP_{,T}}{n_r^2}\right)\mathrm{d}n_r, \quad \tilde{g}(T,n) = \frac{2}{3}\int_0^{n_r}\left(\frac{1}{Rn_c}\frac{P_{,T}}{n_r^2} - \frac{1}{n_r}\right)\mathrm{d}n_r \tag{5.2}$$

where the units have been restored, so that $\tilde{g}(T,n)$ is dimensionless and $h(T,n)$ has the dimension of J/mol. Substituting the EoS (4.10) and its derivative (5.1) into (5.2), we find

$$\tilde{g}(T,n) = \frac{2}{3}\left[I_0(n_r) - I_1(n_r)T_c\sigma' - I_2(n_r)\sigma T_c\alpha' + I_3(n_r)\sigma T_c\rho' + I_4(n_r)\sigma T_c\chi'\right] \tag{5.3}$$

$$h(T,n) = RT_c\left[I_1(n_r)\left(T\sigma' - \sigma\right) + I_2(n_r)\sigma T\alpha' - I_3(n_r)\sigma T\rho' - I_4(n_r)\sigma T\chi'\right] \tag{5.4}$$

where the $I_{k=0,\ldots,4}(n_r)$ denote the integrals

$$I_0 = \int_0^{n_r}\frac{1}{n_r}\left[\left(1+\left(\frac{n_r}{\widehat{b}}\right)^{\lambda/\eta}\right)^{\eta} - 1\right]\mathrm{d}n_r,\ I_1 = \int_0^{n_r}\frac{n_r^{\alpha-2}}{1+\rho n_r+\chi n_r^2}\mathrm{d}n_r$$

$$I_2 = \int_0^{n_r}\frac{n_r^{\alpha-2}\log n_r}{1+\rho n_r+\chi n_r^2}\mathrm{d}n_r,\ (I_3, I_4) = \int_0^{n_r}\frac{(n_r^{\alpha-1}, n_r^{\alpha})}{(1+\rho n_r+\chi n_r^2)^2}\mathrm{d}n_r \tag{5.5}$$

The specific internal energy density $u = U/V$ in (2.8) reads

$$u\left[\mathrm{J}/\mathrm{cm}^3\right] = h(T,n)n_cn_r + (3/2)Rn_cn_rT \tag{5.6}$$

with $h(T,n)$ in (5.4) substituted. Fig. 10 depicts isothermal fits to the internal energy per mole,

$$U[\mathrm{J/mol}] = \frac{u}{n} = h(T,n) + \frac{3}{2}RT \tag{5.7}$$

The fit parameters are the four temperature derivatives α', σ', ρ', χ', which enter linearly in (5.4). All other parameters defining $h(T,n)$ in (5.4) are obtained from the least-squares fits of the pressure isotherms discussed in Section 4.3. The zero-point of the energy scale can be chosen arbitrarily. In Section 2, it is defined by the convention that the ideal gas limit is recovered in the low-density limit. The zero-point of the internal-energy data sets [6] used in the least-squares fits in Fig. 10 is defined by the convention of zero enthalpy at the boiling point. The fits as well as the comparison with the PR equation (see below) are performed by uniformly shifting the data points downwards so that the $3RT/2$ limit

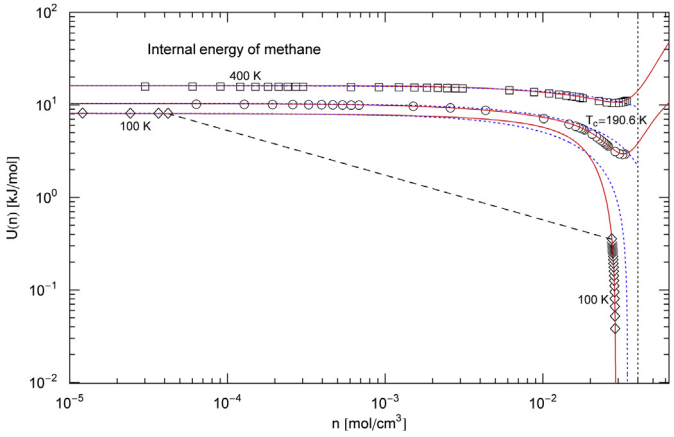

Fig. 10. Internal-energy isotherms of methane. Data points from Ref. [6]; squares/circles/diamonds indicate supercritical/critical/subcritical data points, respectively, at the indicated temperature. The solid red curves depict least-squares fits performed with the internal energy $U(n)$ in (5.7) which is based on the non-cubic EoS (4.10); the fit parameters and determination coefficients are listed in Table 5. The dashed black line connects the saturation points on the subcritical isotherm. The high-density data points of the critical and supercritical isotherms indicate the onset of an internal energy increase above a density of 0.03 mol/cm^3, which is accurately reproduced by the multi-parameter EoS (4.10). The subcritical 100 K isotherm also bends upwards at negative energies (not shown in this log-log plot). The PR approximation of the isotherms is depicted by the dotted blue curves, cf. (5.7) and (5.8). The vertical dotted black line indicates the PR density limit of $n_c/\widehat{p} = 0.040$ mol/cm^3, cf. (4.14) and (4.15), where the pressure singularity of the PR EoS occurs, see Fig. 3.

is recovered at low density. (In Fig. 10, the data sets have been shifted upwards by 1 kJ/mol, so that the lowest energies are still positive, to allow a log-log representation.) Since the fitting parameters α', σ', ρ', χ' enter linearly in (5.7), the derivatives of the least-squares functional linearly depend on these parameters. The least-squares minimization thus amounts to solving a system of four linear equations in the variables α', σ', ρ', χ'. The fit parameters obtained in this way are listed in Table 5 for a subcritical ($T = 100$ K), critical and supercritical ($T = 400$ K) temperature. The data points of the critical and 400 K isotherms in Fig. 10 show the onset of an internal-energy increase at high density, which is accurately reproduced by the fits (solid red curves). The almost vertical slope of the subcritical data set at high density is also well reproduced by the internal energy (5.7) derived from EoS (4.10).

The isochoric heat capacity can be dealt with in like manner, being the temperature derivative of the internal energy. The fitting parameters in this case are the second-order derivatives α'', σ'', ρ'', χ'', which also enter linearly in the derivatives of the least-squares functional and can thus be obtained by linear regression.

The coefficient functions of the Hamiltonian in (5.3) and (5.4) simplify if specialized to the cubic EoS (4.14),

$$\tilde{g}(T,n) = \frac{2}{3}[I_0(n_r) - I_1(n_r)T_c\widehat{a}\widehat{\sigma}'], \quad h(T,n) = RT_cI_1(n_r)(T\widehat{a}\widehat{\sigma}' - \widehat{a}\widehat{\sigma}) \tag{5.8}$$

where $\widehat{\sigma}'(T)$ denotes the temperature derivative of the alpha function in EoS (4.14) and

$$I_0 = \int_0^{n_r} \frac{\widehat{p}}{1-\widehat{p}n_r}\mathrm{d}n_r, \quad I_1 = \int_0^{n_r} \frac{1}{1+\widehat{c}n_r+\widehat{d}n_r^2}\mathrm{d}n_r \tag{5.9}$$

Numerical values of the constants $\widehat{a}, \widehat{c}, \widehat{d}, \widehat{p}$ in (5.8) and (5.9) and analytic expressions for the alpha function $\widehat{\sigma}(T)$ of the PR and SRK EoSs can be found in Section 4.2. The integrals in (5.9) are elementary and so are the coefficient functions in the case of cubic EoSs, see the examples in (2.17)–(2.19).

In Fig. 10, we compare the internal-energy isotherms of the PR EoS (dotted curves defined in (5.7)–(5.9)) with the corresponding isotherms of the non-cubic EoS (4.10) (solid red curves, calculated via (5.4), (5.5) and (5.7)). The internal-energy isotherms obtained from the PR equation are accurate up to about the critical density but fail to fit the high-density data points at critical and subcritical temperatures, whereas the isotherms calculated from the multi-parameter EoS (4.10) give uniformly accurate fits to all three data sets.

6. Results, discussion and conclusion

We have explained the reconstruction of the effective Hamiltonian from a thermal EoS, cf. Section 2. This Hamiltonian explicitly depends on temperature and particle density and satisfies an equilibrium condition, cf. Section 3, so that the partition function defines a genuine equilibrium system with entropy variable $S(U,N,V)$ satisfying $S_{,U} = 1/T$ and $S_{,V} = P/T$, the pressure coinciding with the prescribed EoS.

Once the effective Hamiltonian is known, one can calculate the partition function, caloric EoS and entropy variable, cf. (2.9) and (2.14). The chemical potential is found via the entropy derivative $S_{,N} = -\mu/T$, cf. (2.13) and (3.13). All other thermodynamic variables such as heat capacities and compressibilities are obtained from these quantities by using standard equilibrium identities, cf. (3.14). Explicit formulas to calculate the effective Hamiltonian from a prescribed EoS have been derived in Section 2.2; the integrals involved are elementary for cubic equations, and the Hamiltonians of the SRK and PR equations are stated in (2.18) and (2.19).

As cubic EoSs tend to be inaccurate at high density (see Sections 4.3 and 5 and the PR approximations of the isotherms in Figs. 1–8 and 10), a non-cubic multi-parameter equation has been proposed in Section 4.1,

$$P(n,T) = Rn_cT_c\left[n_rT_r\left(1+\left(\frac{n_r}{\widehat{b}}\right)^{\lambda/\eta}\right)^{\eta} - \frac{n_r^{\alpha(T)}\sigma(T)}{1+\rho(T)n_r+\chi(T)n_r^2}\right] \tag{6.1}$$

The subscripts indicate critical and reduced temperatures and densities. Like cubic equations, this EoS consists of a repulsive and attractive term. The latter is similarly structured as in the cubic EoS (4.14), apart from the non-integer exponent $\alpha(T)$, so that the three conditions $P_c = P(n_c,T_c)$ and $P_{,n} = P_{,n,n} = 0$ at the critical point can be solved explicitly for the amplitudes $\sigma(T_c)$, $\rho(T_c)$, $\chi(T_c)$. The basic difference to cubic EoSs is the repulsive term, which is non-singular at high density and depends on real exponents λ and η. The

Table 5
Fitting parameters of the internal-energy isotherms of methane in Fig. 10. Recorded are the temperature derivatives of the exponent $\alpha(T)$ and amplitudes $\sigma(T)$, $\rho(T)$, $\chi(T)$ in the attractive term of the non-cubic EoS (4.10), at a subcritical, critical and supercritical temperature. The parameters are obtained from least-squares fits of the internal energy (5.7) based on EoS (4.10). R^2 is the determination coefficient of the fits.

T[K]	$\alpha'(T)$	$\sigma'(T)$	$\rho'(T)$	$-\chi'(T)$	$1-R^2$
100	1.1841×10^{-3}	5.3045×10^{-4}	3.4160×10^{-4}	2.3126×10^{-4}	4.5×10^{-8}
190.56	4.1478×10^{-3}	7.3200×10^{-3}	1.2480×10^{-3}	2.1520×10^{-4}	2.8×10^{-4}
400	2.7228×10^{-3}	1.1565×10^{-2}	1.5112×10^{-3}	1.6057×10^{-4}	7.0×10^{-4}

effective Hamiltonian obtained from EoS (6.1) is assembled in Section 5.

The EoS (6.1) has been tested by performing least-squares fits to isothermal high-pressure data sets of nitrogen, carbon monoxide, methane, carbon dioxide, methanol, water, hydrogen and helium, depicted in Figs. 1–8, cf. Section 4.3. The critical pressure isotherms defined by EoS (6.1) depend on four positive fit parameters $\widehat{b}$, λ, η, $\alpha(T_c)$, recorded in Table 2, the remaining three parameters $\sigma(T_c)$, $\rho(T_c)$, $\chi(T_c)$ are determined by the above conditions at the critical point.

The parameters $\widehat{b}$, λ, η of EoS (6.1), obtained from the fit of the critical isotherm, define the repulsive term of the EoS and are temperature independent [45], so that they remain valid for sub- and supercritical isotherms as well. The latter thus require four (temperature dependent) fit parameters $\alpha(T)$, $\sigma(T)$, $\rho(T)$, $\chi(T)$ defining the attractive term in (6.1), which are listed in Table 3. In effect, the least-squares fits in Figs. 1–8 are obtained by varying four parameters, either $\widehat{b}$, λ, η, $\alpha(T_c)$ in the case of critical isotherms or α, σ, ρ, χ at non-critical temperatures. The isothermal data sets used for the fits in Figs. 1–8 cover five pressure decades, up to 1 GPa [6]. As is evident from the figures, the fitted pressure isotherms (solid red curves) are uniformly accurate over the measured pressure range, for critical, sub- and supercritical temperatures alike. The determination coefficients of the least-squares fits depicted in Figs. 1–8 are listed in Tables 2 and 3. Analogous to the alpha function of the cubic PR equation, cf. Section 4.2, the temperature dependent exponent and amplitudes $\alpha(T)$, $\sigma(T)$, $\rho(T)$, $\chi(T)$ in the attractive term of EoS (6.1) can be specified as analytic functions instead of being treated as fitting parameters, cf. Section 4.4. In the vicinity of the critical temperature, these functions admit power series expansions. We studied the temperature dependence of water pressure isotherms, calculated the series coefficients, cf. Fig. 9 and Table 4, and obtained the temperature parametrization of the EoS of water in the 300 K – 1200 K range where the series expansions apply.

The effective Hamiltonian of EoS (6.1) determines the internal-energy variable (5.7) which has been put to test by performing least-squares fits to methane data sets, cf. Section 5. Since the Hamiltonian depends on the temperature derivative of EoS (6.1), the fit parameters of the internal energy are the four temperature derivatives α', σ', ρ', χ' of the exponent and the amplitudes in the attractive term of EoS (6.1). All other parameters are predetermined by the fits of the pressure isotherms. The internal-energy isotherms of methane are depicted in Fig. 10, at critical, sub- and supercritical temperatures. The data sets cover the same extended density range as the methane pressure isotherms in Fig. 3, and the least-squares fits (solid red curves) are quite accurate, especially at high density; the fitting parameters, obtained by linear regression, and the determination coefficients are listed in Table 5.

In Figs. 1–8 and 10, the isotherms of the multi-parameter EoS (6.1) are compared with the corresponding isotherms of the cubic PR equation, cf. Section 4.2. As illustrated by the figures, the PR EoS is quite efficient to model isotherms up to about the critical density and, for supercritical temperatures, even above that. It is essentially a universal equation depending, apart from the critical temperature and density, only on one compound-specific parameter, the acentric factor in the alpha function of the EoS. Its simplicity and wide applicability makes it attractive for engineering applications. However, as is also evident from the figures, there are limits regarding its accuracy and applicability in the high-density/high-pressure regime, especially at critical and subcritical temperatures. First, the pressure isotherms at critical temperature, which do not even depend on the uncertain alpha function, become inaccurate at the critical density if the critical compressibility factor Z_c of the fluid deviates from the assumed universal Z_c of the PR equation, cf. Eq. (4.15) and Table 1. Second, above the critical density, there is a straight power-law segment visible in the data sets of the critical pressure isotherms. (Straight segments in log-log plots indicate power-law slopes.) These straight power-law segments extend to the highest measured pressure, see Figs. 1–8, and are not reproduced by the critical PR isotherms (indicated by dotted curves in the figures) which show substantial curvature in log-log plots and terminate in a pressure singularity. This singularity predicted by the PR and other cubic EoSs is not evidenced in any of the data sets in Figs. 1–8, in contrast to the power-law segment emerging in all figures.

The sub- and supercritical isotherms of the PR EoS depend on the choice of the alpha function in the attractive term of the EoS, cf. Section 4.2. This is an analytic function of temperature, depending on compound-specific constants sometimes correlated with the acentric factor. There is no consensus on the actual structure of this function, see Table 1 of Ref. [5] for suggestions of closed analytic expressions in this regard. The alpha function used in the plots in Figs. 1–8 and 10 is stated at the end of Section 4.2. The subcritical data points of the liquid phase in Figs. 1–8 define an extremely steep slope of the pressure isotherms, which is not well reproduced by the PR EoS.

As is the case for pressure isotherms, the PR isotherms of the internal energy of methane in Fig. 10 (dotted blue curves) are accurate up to the critical point and deviate from the data points for higher densities. The data sets of the supercritical and critical isotherms show the onset of an energy increase at high density not reproduced by the PR isotherms. The latter are monotonously decreasing, terminating at the limit density defined by the pressure singularity (indicated by the vertical dotted line in Fig. 10). The subcritical PR isotherm (dotted blue curve) does not match the data points at high density either.

One can thus draw the following conclusion. The PR EoS with an alpha function correlated with the acentric factor is easy to apply and gives reasonably accurate predictions of thermodynamic functions at low and intermediate densities just by specifying the acentric factor. But the PR equation is approximative by design, due to the assumed universal compressibility factor, uncertain alpha function and correlation with the acentric factor, and is not suitable for the high-density/high-pressure regime.

The multi-parameter EoS (6.1) is more difficult to apply, since the parameters have to be calculated by least-squares fits. But this non-cubic EoS can accurately reproduce the measured high-density data sets and predict the continuation of isotherms beyond the PR singularity, as demonstrated for pressure isotherms in Figs. 1–8 and internal-energy isotherms in Fig. 10.

List of symbols and abbreviations

The ordering of the symbols is according to first appearance in the text.

Section 1

PR EoS	Peng-Robinson equation of state
SRK EoS	Soave-Redlich-Kwong equation of state

Section 2

$\mathrm{d}\rho(p)$	spectral density, see (2.1)
$H(p;T,n)$	effective Hamiltonian
p	particle momentum
$n = N/V$	particle density
σ	spin degeneracy
$\alpha(T,n)$	fugacity parameter
$\beta = 1/T$	inverse temperature
$u = U/V$	internal energy density

Z, $\xi = \log Z/V$ partition function
m particle mass
$g(T,n)$, $h(T,n)$, $\tilde{g}(T,n) = \log(2mg(T,n))$ coefficient functions of the effective Hamiltonian
$g_{,n}$, $h_{,T}$ derivatives are indicated by subscript commas followed by the respective variable; primes are also used to denote temperature derivatives
P pressure
μ chemical potential
C_V isochoric heat capacity
$s(T,n) = S/V$ specific entropy density
F Helmholtz free energy

Section 3
$f(x)$ integral kernel of the partition function
$Z_{\mathrm{F,B}}$, $\mathrm{d}\rho_{\mathrm{F,B}}(p)$ F and B subscripts referring to Fermi and Bose statistics
κ_T isothermal compressibility
α_{exp} isobaric expansion coefficient
C_P isobaric heat capacity
κ_S adiabatic compressibility

Section 4.1
$n[\mathrm{mol/cm^3}]$ molar density
$V_{\mathrm{c}} = 1/n_{\mathrm{c}}$ critical molar volume
R universal gas constant
$Z_{\mathrm{c}} = P_{\mathrm{c}}V_{\mathrm{c}}/(RT_{\mathrm{c}})$ critical compressibility factor, the subscript c denoting critical values
$T_{\mathrm{r}} = T/T_{\mathrm{c}}$, $n_{\mathrm{r}} = n/n_{\mathrm{c}}$ subscript r denoting reduced values
λ, η,$\widehat{b}$ exponents and amplitude parametrizing the repulsive term of the non-cubic multi-parameter EoS (4.10)
$\alpha(T)$, $\sigma(T)$, $\rho(T)$, $\chi(T)$ temperature dependent exponent and amplitudes defining the attractive term of the EoS (4.10)
$\alpha_{\mathrm{c}} = \alpha(T_{\mathrm{c}})$, $\widehat{a} = \sigma(T_{\mathrm{c}})$, $\widehat{c} = \rho(T_{\mathrm{c}})$, $\widehat{d} = \chi(T_{\mathrm{c}})$ exponent and amplitudes in EoS (4.10) at the critical temperature

Section 4.2
$\widehat{p}$, $\widehat{a}$, $\widehat{c}$, $\widehat{d}$ constant amplitudes in the cubic EoS (4.14)
$\widehat{\sigma}(T) = \sigma(T)/\widehat{a}$ alpha function in the attractive term of the cubic EoS (4.14)
ω acentric factor
$\Omega(\omega)$ empirical function of the acentric factor, used to parametrize the alpha function $\widehat{\sigma}(T)$ of the cubic EoS (4.14)

Section 4.3
R^2 determination coefficient of a least-squares fit, see Table 2

Section 4.4
c_i expansion coefficients of the analytic functions $\alpha(T)$,$\sigma(T)$,$\rho(T)$,$\chi(T)$ defining the attractive term of EoS (4.10)

Section 5
α', σ', ρ', χ' temperature derivatives of the exponent and amplitudes in the non-cubic EoS (4.10)
$I_{k=0,\ldots,4}$ integrals stated in (5.5) defining the Hamiltonian of the non-cubic EoS (4.10)
$\widehat{\sigma}'$ temperature derivative of the alpha function of the cubic EoS (4.14)

References

[1] L.D. Landau, E.M. Lifshitz, Statistical Physics, third ed., Pergamon, Oxford, 1980.
[2] D.A. McQuarrie, Statistical Mechanics, Harper & Row, New York, 1976.
[3] G. Kontogeorgis, B. Maribo-Mogensen, K. Thomsen, Fluid Phase Equilib. 462 (2018) 130.
[4] B.E. Poling, J.M. Prausnitz, J.P. O'Connell, The Properties of Gases and Liquids, fifth ed., McGraw-Hill, Boston, 2009.
[5] J.S. Lopez-Echeverry, S. Reif-Acherman, E. Araujo-Lopez, Fluid Phase Equilib. 447 (2017) 39.
[6] E.W. Lemmon, M.O. McLinden, D.G. Friend, Thermophysical properties of fluid systems, in: P.J. Linstrom, W.G. Mallard (Eds.), NIST Chemistry WebBook, NIST Standard Reference Database Nr. 69, NIST, Gaithersburg, MD, 2019. https://webbook.nist.gov/chemistry/fluid/.
[7] P.M. Mathias, T.W. Copeman, Fluid Phase Equilib. 13 (1983) 91.
[8] R. Stryjek, J.H. Vera, Can. J. Chem. Eng. 64 (1986) 820.
[9] W. Sheng, B.C.-Y. Lu, Fluid Phase Equilib. 56 (1990) 71.
[10] G. Soave, Chem. Eng. Sci. 39 (1984) 357.
[11] G. Soave, Fluid Phase Equilib. 82 (1993) 345.
[12] K.A.M. Gasem, W. Gao, Z. Pan, R.L. Robinson, Fluid Phase Equilib. 181 (2001) 113.
[13] A. Kumar, R. Okuno, Ind. Eng. Chem. Res. 53 (2014) 440.
[14] R. Privat, M. Visconte, A. Zazoua-Khames, J.-N. Jaubert, R. Gani, Chem. Eng. Sci. 126 (2015) 584.
[15] L.A. Forero, J.A. Velásquez, Fluid Phase Equilib. 418 (2016) 74.
[16] P. Mahmoodi, M. Sedigh, J. Supercrit. Fluids 112 (2016) 22.
[17] P. Mahmoodi, M. Sedigh, J. Supercrit. Fluids 120 (2017) 191.
[18] P. Mahmoodi, M. Sedigh, Fluid Phase Equilib. 436 (2017) 69.
[19] Y. Le Guennec, S. Lasala, R. Privat, J.-N. Jaubert, Fluid Phase Equilib. 427 (2016) 513.
[20] Y. Le Guennec, R. Privat, S. Lasala, J.-N. Jaubert, Fluid Phase Equilib. 445 (2017) 45.
[21] F. Yang, Q. Liu, Y. Duan, Z. Yang, Chem. Eng. Sci. 192 (2018) 565.
[22] A. Pina-Martinez, R. Privat, J.-N. Jaubert, D.-Y. Peng, Fluid Phase Equilib. 485 (2019) 264.
[23] B.A. Younglove, J. Phys. Chem. Ref. Data 11 (Suppl. 1) (1982).
[24] B.A. Younglove, J.F. Ely, J. Phys. Chem. Ref. Data 16 (1987) 577.
[25] U. Setzmann, W. Wagner, J. Phys. Chem. Ref. Data 20 (1991) 1061.
[26] R. Span, W. Wagner, Int. J. Thermophys. 18 (1997) 1415.
[27] A. Gonzalez Perez, C. Coquelet, P. Paricaud, A. Chapoy, Fluid Phase Equilib. 440 (2017) 19.
[28] O. Kunz, W. Wagner, J. Chem. Eng. Data 57 (2012) 3032.
[29] P. Aursand, M. Gjennestad, E. Aursand, M. Hammer, Ø. Wilhelmsen, Fluid Phase Equilib. 436 (2017) 98.
[30] R. Tomaschitz, Physica A 483 (2017) 438.
[31] R. Tomaschitz, Physica A 489 (2018) 128.
[32] R. Tomaschitz, Eur. Phys. J. B 91 (2018) 115.
[33] E. Holleran, Fluid Phase Equilib. 251 (2007) 29.
[34] R. Privat, Y. Privat, J.-N. Jaubert, Fluid Phase Equilib. 282 (2009) 38.
[35] M.F. Pérez-Polo, M. Pérez-Molina, E. Fernández Varó, J. Gil Chica, Fluid Phase Equilib. 473 (2018) 262.
[36] N.C. Patel, A.S. Teja, Chem. Eng. Sci. 37 (1982) 463.
[37] N.C. Patel, Int. J. Thermophys. 17 (1996) 673.
[38] J.O. Valderrama, Ind. Eng. Chem. Res. 42 (2003) 1603.
[39] S. Esmaeili, S. Maaref, Fluid Phase Equilib. 473 (2018) 112.
[40] M.A. Trebble, P.R. Bishnoi, Fluid Phase Equilib. 29 (1986) 465.
[41] M.A. Trebble, P.R. Bishnoi, Fluid Phase Equilib. 35 (1987) 1.
[42] P.H. Salim, M.A. Trebble, Fluid Phase Equilib. 65 (1991) 59.
[43] T.E. Daubert, R.P. Danner, H.M. Sibel, C.C. Stebbins, Physical and Thermodynamic Properties of Pure Chemicals: Data Compilation, Taylor & Francis, Washington, D.C., 1997.
[44] T.O. Kvålseth, Am. Statistician 39 (1985) 279.
[45] V. Kalikhman, D. Kost, I. Polishuk, Fluid Phase Equilib. 293 (2010) 164.